

Modelling damage and permanent strain in fibre-reinforced composites under in-plane fatigue loading

W. Van Paepegem* and J. Degrieck

Ghent University, Dept. of Mechanical Construction and Production,
Sint-Pietersnieuwstraat 41, 9000 Gent, Belgium

Abstract

The vast majority of the fatigue models for fibre-reinforced composites is limited to one-dimensional loading conditions. Due to the heterogeneous and anisotropic nature of composites, the extension of these models towards multi-axial fatigue loading conditions is not straightforward. This paper presents a phenomenological residual stiffness model that predicts the stiffness degradation and (possible) permanent strain in fibre-reinforced polymers under in-plane fatigue loading. The model takes into account the actual stress state in each material point and does not make any assumptions about geometry or boundary conditions of the fatigue loaded specimen. As the presented model has been developed within a larger research programme, the emphasis in this paper lies on the theoretical modelling framework, rather than on an in-depth validation of the model which would require much more detail about the close feedback between experimental data and finite element simulations. Therefore the development of the stress-strain-damage relationships and the damage growth rate equations is explained thoroughly and a few finite element results are presented for plain woven glass/epoxy composites.

Keywords A: Polymer-matrix composites (PMCs); B: Fatigue; C: Damage mechanics; C: Finite element analysis (FEA).

Nomenclature

c_i ($i = 1, \dots, 6$)	material constants for glass/epoxy material
C_{ij}	homogenized stiffness tensor of the undamaged material
D	scalar damage variable
D_{ij} ($i, j = 1, 2$)	in-plane damage variables
E_0	longitudinal stiffness modulus
E_{11}	stiffness modulus in warp direction of the glass/epoxy lamina
E_{22}	stiffness modulus in weft direction of the glass/epoxy lamina
ε	one-dimensional applied strain
ε_{ij}	strain tensor
ε_{ii}^p ($i = 1, 2$)	permanent strain
G_{12}	shear modulus
ν_{12}	Poisson coefficient
N	number of cycles
R	stress ratio ($= \sigma_{\min}/\sigma_{\max}$)
S	shear strength of glass/epoxy lamina

* Corresponding author (Fax: +32-(0)9-264.35.87, E-mail: Wim.VanPaepegem@rug.ac.be).

σ	one-dimensional applied nominal stress
$\tilde{\sigma}$	one-dimensional effective stress ($\tilde{\sigma} = \sigma / (1 - D)$)
σ_{ij}	stress tensor
Σ	one-dimensional fatigue failure index
Σ_{ij} (i, j = 1,2)	in-plane fatigue failure indices
u_{\max}	maximum prescribed displacement in bending fatigue setup
X_T	tensile strength in warp direction of glass/epoxy lamina
X_C	compression strength in warp direction of glass/epoxy lamina
Y_T	tensile strength in weft direction of glass/epoxy lamina
Y_C	compression strength in weft direction of glass/epoxy lamina
W_D	dissipated energy during one fatigue loading cycle
$[\#0^\circ]_8$	stacking sequence of eight glass/epoxy laminae, the weft direction being aligned with the loading direction in bending
$[\#45^\circ]_8$	stacking sequence of eight glass/epoxy laminae, the weft (and warp) direction under 45° with the loading direction in bending

1. Introduction

Fibre-reinforced composites are used in many fatigue-critical applications, but their heterogeneous and anisotropic nature complicates the development of adequate models for simulating their fatigue behaviour under multi-axial loading conditions. This paper presents the development of a phenomenological residual stiffness model which predicts the stiffness degradation and possible accumulation of permanent strain in fibre-reinforced polymers under generalized in-plane fatigue loading. The existing fatigue models for fibre-reinforced composites can generally be classified into [1]: (i) fatigue life models (S-N curves), (ii) damage accumulation models ('mechanistic models'), and (iii) phenomenological residual stiffness/strength models. The scope of most models is limited to one-dimensional fatigue loading, although some models have been applied to multi-axial fatigue loading.

In the category of fatigue life models, the multi-axial loading problem is often handled by introducing a static failure criterion (e.g. Tsai-Wu, Tsai-Hill) and replacing the static strengths with the fatigue strengths in the criterion. This approach was followed by Lawrence Wu [2], Jen and Lee [3-4] and Philippidis and Vassilopoulos [5]. The drawback of this approach is that the fatigue strengths must be determined experimentally for different stress amplitudes, stress ratios and bi-axiality ratios. This requires a large experimental input of S-N curves which represent directly the perceived nature of fatigue in terms of experimental results, but give no indication of the mechanisms of fatigue damage, of the presence or behaviour of cracks, or of changes in the characteristics of the material as a consequence of the fatigue process.

Well-known mechanistic models for multi-axial fatigue loading are the continuum damage models by Talreja [6-8], Allen et al. [9-12] and Sedrakian et al. [13-14]. Recently, Shokrieh and Lessard [15-20] proposed a so-called 'generalized residual material property degradation model' for unidirectionally reinforced laminates which uses Hashin-type fatigue failure criteria to determine the damage mode and consequently reduces the corresponding elastic properties.

In this paper, the phenomenological residual stiffness approach is adopted to simulate stiffness degradation, stress redistribution and permanent strain in fibre-reinforced polymers under generalized in-plane loading. The presence of each of these phenomena was clearly indicated by the experimental results which were obtained from displacement-controlled

bending fatigue tests on plain woven glass/epoxy composites. The experimental results are discussed in the following paragraph.

2. Experimental setup and material

2.1. Experimental setup

The fatigue tests were performed with a *displacement-controlled* bending device. It is schematically shown in Figure 1.

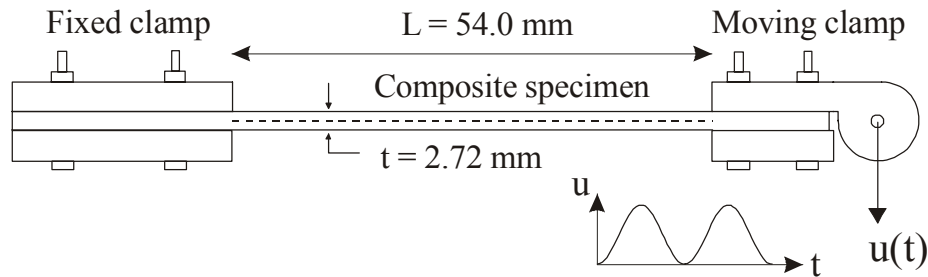


Figure 1 Schematic representation of the experimental bending fatigue setup.

The amplitude of the prescribed displacement $u(t)$ at the moving clamp is denoted as u_{\max} [millimeter]. This amplitude is constant throughout the whole fatigue test, but for each separate test its value can be adjusted by a mechanism with crank and connecting-rod. The force necessary to bend the specimen is measured by a strain gauge bridge on the connecting-rod. The amplitude of this force, corresponding with the maximum displacement u_{\max} , is denoted as F [Newton]. It is important to mention that this force F represents the global force to pull the specimen into its maximum deformed position, but no local strains were measured on the surface of the composite specimen itself. Further, the bending device has been equipped with optical instruments to measure at regular intervals the out-of-plane displacement profile of the composite specimen in its maximum deformed state [21-22]. The following discussion will be limited to fatigue tests in single-sided bending where the composite specimen only bends in one direction. Fully-reversed bending tests have been discussed in [23].

2.2. Material

The material used was an epoxy matrix (Araldite LY 556, Ciba-Geigy) reinforced with plain woven glass fabric (Roviglass R420, Syncoglas). The fabric was stacked in eight layers and two different stacking sequences were chosen. For the first stacking sequence, the warp direction of all eight layers was aligned with the bending direction (denoted as $[\#0^\circ]_8$, where the hash mark '#' refers to the fabric reinforcement type). For the second stacking sequence, the angle between the warp direction of all layers and the bending direction was 45° (denoted as $[\#45^\circ]_8$). The two stacking sequences are supposed to represent two fundamentally different stress states. The bending of the $[\#0^\circ]_8$ stacking sequence results in a quasi one-dimensional loading of the laminate, with large stresses along the longitudinal fibre direction. In the $[\#45^\circ]_8$ stacking sequence, the load is sustained by a combined state of normal stresses in the two fibre directions of the fabric, and shear stresses.

All composite specimens were manufactured using a vacuum-assisted resin transfer moulding technique in a closed steel mould. After curing they had a thickness of 2.72 mm. The fibre

volume fraction V_f was 0.48. The samples were cut to dimensions of 145 mm long by 30 mm wide on a water-cooled diamond saw.

The in-plane elastic properties of the $[\#0^\circ]_8$ composite laminates were determined using the dynamic modulus identification method described by Sol et al. [24-25]. They are listed in Table 1.

Table 1 Measured in-plane elastic properties of the $[\#0^\circ]_8$ composite laminates.

E_{11} [GPa]	24.57
E_{22} [GPa]	23.94
ν_{12} [-]	0.153
G_{12} [GPa]	4.83

There is a slight difference between the measured values of E_{11} and E_{22} . This must be due to fabrication or measurement circumstances, because the plain woven fabric is balanced in its warp and weft direction. Therefore, the mean value of E_{11} and E_{22} has been used for all numerical analyses.

Finally, the mean values of the in-plane static strengths are listed in Table 2. X_T and X_C are the tensile and compressive static strength in the warp direction, Y_T and Y_C are the tensile and compressive static strength in the weft direction, and S is the static shear strength. As the fabric is plain woven, it is assumed again that $Y_T = X_T$ and $Y_C = X_C$.

Table 2 Measured in-plane static strengths of the $[\#0^\circ]_8$ composite laminates.

X_T [MPa]	390.7
X_C [MPa]	345.1
Y_T [MPa]	390.7
Y_C [MPa]	345.1
S [MPa]	100.6

2.3. Typical experimental results

Figure 2 shows the force-cycle history for a $[\#0^\circ]_8$ and $[\#45^\circ]_8$ specimen, subjected to single-sided bending with $u_{\max} = 34.4$ mm. The abscissa contains the number of cycles; the ordinate axis shows for each loading cycle the corresponding maximum value of the force F [Newton] as measured by the strain gauge bridge on the connecting-rod of the bending device.

The $[\#0^\circ]_8$ specimen degrades gradually in the early loading cycles, but its stiffness is reduced significantly after about 40,000 cycles. The initial force on the $[\#45^\circ]_8$ specimen is smaller, because its (bending) stiffness is lower. However, after about 50,000 cycles, its remaining stiffness has become larger than that of the $[\#0^\circ]_8$ specimen. Of course, the ratio of the surface strain to the ultimate strain is different for the two specimen types. This can be easily demonstrated by a structural analysis of the laminate when a constant curvature κ_x is imposed. The Tsai-Wu failure criterion will reach its failure value much earlier for the $[\#0^\circ]_8$ specimen than for the $[\#45^\circ]_8$ specimen, because the stresses, resulting from the imposed curvature, are smaller for the $[\#45^\circ]_8$ specimen.

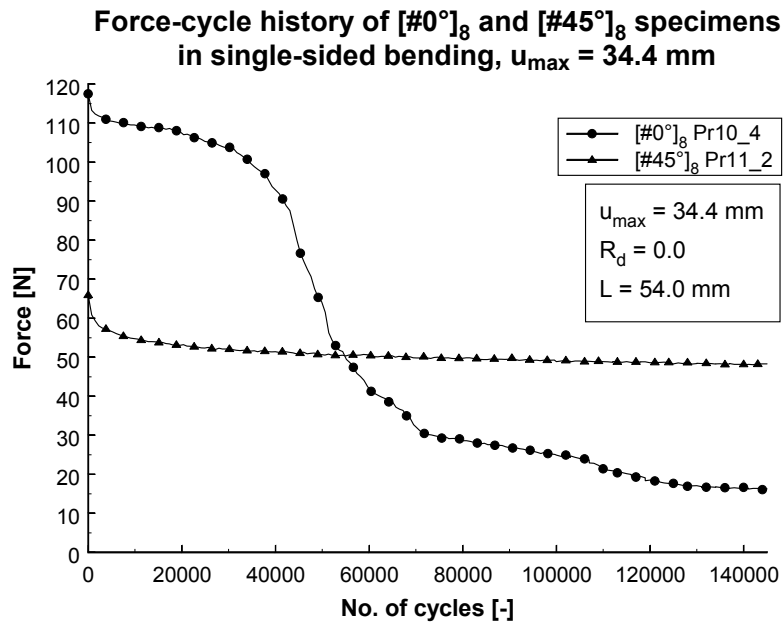


Figure 2 Force-cycle histories for $[\#0^\circ]_8$ and $[\#45^\circ]_8$ specimens (single-sided bending, $u_{\max} = 34.4$ mm).

Further, it was observed that the out-of-plane displacement profile of the $[\#0^\circ]_8$ specimen (which was always recorded in the maximum deformed state) drastically changed during loading time from a smoothly curved profile at the first loading cycles, towards a straight profile with a sort of ‘hinge’ at the clamped cross-section. On the other hand, the out-of-plane displacement profile of the $[\#45^\circ]_8$ specimen remained quasi unchanged during the whole loading time, but these latter specimens showed a considerable permanent deformation under large prescribed displacements. Indeed, when u_{\max} was large, a substantial permanent deformation did remain after removing the clamps from the $[\#45^\circ]_8$ specimens, while this was barely the case for the $[\#0^\circ]_8$ specimens. For each $[\#45^\circ]_8$ specimen, the permanent deformation was also measured after 3 days, 7 days and one month. However, no recovery of the permanent deformation could be observed.

Figure 3 shows a picture of three $[\#45^\circ]_8$ specimens Pr06_3, Pr06_4 and Pr06_5, after having been subjected to a prescribed displacement u_{\max} of 38.9 mm for about 900,000 loading cycles. The fourth specimen at the right-hand side of the picture is an undamaged specimen for comparison purpose. At the lower specimen ends, the permanent deformation is about 18 % of the prescribed displacement amplitude u_{\max} .

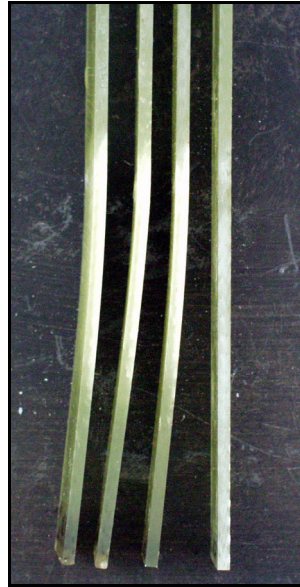


Figure 3 Permanent deformation of $[\#45^\circ]_8$ specimens after removing the clamps.

This phenomenon of permanent deformation might be due to matrix crazing. The prevailing stresses in the $[\#45^\circ]_8$ specimens are shear stresses which induce much friction. Matrix debris is formed and is accumulated between the crack faces. This excess material prevents the matrix cracks from closing completely when the applied displacement returns to zero. When removing the clamps, the cracks in the $[\#45^\circ]_8$ specimens remain partially opened. For the $[\#0^\circ]_8$ specimens on the other hand, the matrix cracks are perpendicular to the loading direction and are opened and closed during each loading cycle. A similar explanation has been proposed by Wevers et al. [26-27] who studied the formation of small matrix cracks at a $\pm 45^\circ$ angle to the full thickness matrix cracks in carbon/epoxy composites.

Such permanent deformations are difficult to observe when specimens are loaded in uni-axial tension and/or compression because of the very small in-plane displacements, but are easy to measure in bending, because the resulting out-of-plane displacements are much larger.

Summarized, in order to simulate all experimentally observed phenomena, the fatigue damage model should account for: (i) stiffness degradation (decreasing bending force), (ii) stress redistribution (changing out-of-plane displacement profiles), and (iii) accumulation of permanent strain.

As the bending fatigue of the $[\#0^\circ]_8$ stacking sequence can be considered as a quasi one-dimensional loading, previous efforts of the authors have been concentrated on developing a one-dimensional fatigue damage model for single-sided bending of the $[\#0^\circ]_8$ specimens [28-30]. Later, the one-dimensional model was extended for fully-reversed bending of the $[\#0^\circ]_8$ specimens [23,31]. In the next paragraph, the basic equations of this one-dimensional fatigue model for single-sided bending are shortly reviewed. Next in this paper, the fatigue model will be extended for generalized in-plane fatigue loading conditions.

3. Review of the one-dimensional model for single-sided bending

The one-dimensional fatigue model for single-sided bending is based on the phenomenological residual stiffness approach. Stress and strain are related by the commonly used equation in continuum damage mechanics:

$$\tilde{\sigma} = \frac{\sigma}{1-D} = E_0 \cdot \varepsilon \quad (1)$$

where $\tilde{\sigma}$ is the effective stress, σ is the applied nominal stress, ε is the nominal strain, E_0 is the undamaged Young's modulus and D is a measure for the fatigue damage. The scalar damage variable D , defined as $D = 1 - E/E_0$, is a macroscopic measure for the fatigue damage, since the structural changes on the microscopic scale (matrix cracks, fibre/matrix interface failure,...) are characterized by a macroscopic reduction of the stiffness. The value of D is lying between zero (virgin material state) and one (final failure).

The remaining equation to complete the fatigue model is the damage evolution law dD/dN which predicts the damage increment per cycle. Of course, this law must be a function of the stress amplitude σ , because the larger the applied stress amplitude, the faster the damage will initiate and grow. However, the use of the nominal stress amplitude σ does not give any indication about the relation between the damage and the actual residual strength. Therefore, a new damage-dependent stress measure $\Sigma(\sigma, D)$ has been defined.

To that purpose the nominal stress σ has been replaced by the effective stress $\tilde{\sigma}$ ($= \sigma/(1-D)$) in the one-dimensional Tsai-Wu criterion and the corresponding *fatigue failure index* $\Sigma(\sigma, D)$ has been calculated from:

$$\left(\frac{\sigma}{\Sigma \cdot (1-D)} \right)^2 \frac{1}{X_T \cdot |X_C|} + \frac{\sigma}{\Sigma \cdot (1-D)} \left(\frac{1}{X_T} - \frac{1}{|X_C|} \right) - 1 = 0 \quad (2)$$

The roots of Equation (2) are: $\Sigma = \sigma/[X_T \cdot (1-D)]$ and $\Sigma = -\sigma/[|X_C| \cdot (1-D)]$. Depending on the sign of the nominal stress σ , the *fatigue failure index* $\Sigma(\sigma, D)$ can be written as:

$$\Sigma(\sigma, D) = \frac{\tilde{\sigma}}{X} = \frac{\sigma}{1-D} \stackrel{\text{Eq.(1)}}{=} \frac{E_0 \cdot \varepsilon}{X} \quad \begin{cases} X = X_T & \text{if } \sigma \geq 0 \\ X = -|X_C| & \text{if } \sigma < 0 \end{cases} \quad (3)$$

In fact, for one-dimensional loading, the *fatigue failure index* $\Sigma(\sigma, D)$ could be simply defined as the ratio of the effective stress $\tilde{\sigma}$ to the static strength, without making any mention of the Tsai-Wu failure criterion. However, the Tsai-Wu criterion will be used to extend the definition of the *fatigue failure index* to multi-axial loading.

This *fatigue failure index* Σ has then been used as the driving force for the damage evolution law dD/dN . The fatigue model distinguishes between a growth rate dD/dN for tensile stresses ($\sigma \geq 0$) and one for compressive stresses ($\sigma < 0$) [28-30]:

$$\frac{dD}{dN} = \begin{cases} \underbrace{c_1 \cdot \Sigma \cdot \exp\left(-c_2 \frac{D}{\sqrt{\Sigma}}\right)}_{\text{initiation}} + \underbrace{c_3 \cdot D \cdot \Sigma^2 \cdot [1 + \exp(c_5(\Sigma - c_4))]}_{\text{propagation}} & \text{if } \sigma \geq 0 \\ \underbrace{\left[c_1 \cdot \Sigma \cdot \exp\left(-c_2 \frac{D}{\sqrt{\Sigma}}\right) \right]^3}_{\text{initiation}} + \underbrace{c_3 \cdot D \cdot \Sigma^2 \cdot \left[1 + \exp\left(\frac{c_5}{3}(\Sigma - c_4)\right) \right]}_{\text{propagation}} & \text{if } \sigma < 0 \end{cases} \quad (4)$$

Both growth rate equations consist of two terms, separately accounting for damage initiation and damage propagation. If damage is very small, the second term is negligible ($D \approx 0$) and

only the first initiation term is acting, while for larger values of D , the exponential function in the first term forces this term to diminish, while the second term is increasingly dominating. The damage initiation rate is different in tension and compression, because it was observed from the experimental fatigue tests that the compressive damage initiation rate is much smaller.

The parameters c_i ($i = 1, \dots, 5$) have been determined from a “standard” bending fatigue test with the displacement amplitude $u_{\max} = 30.4$ mm [28]. Their values are listed in Table 3 and will be used for all subsequent simulations.

Table 3 Material constants c_i ($i = 1, \dots, 5$).

c_1 [1/cycle]	0.002
c_2 [-]	30.0
c_3 [1/cycle]	$4.0 \cdot 10^{-6}$
c_4 [-]	0.85
c_5 [-]	93.0

The one-dimensional fatigue damage model (4) has been largely validated for the $[\#0^\circ]_8$ stacking sequence [23,28-30,35]. Typical results of experimental and simulated force-cycle histories for a wide range of fatigue lives are shown in Figure 4. All finite element simulations were performed with the same set of material constants c_i ($i = 1, \dots, 5$) (see Table 3). Due to the introduction of the *fatigue failure index* Σ , both stiffness degradation and final failure can be predicted.

Experimental and simulated force-cycle history for $[\#0^\circ]_8$ specimens in single-sided bending, $u_{\max} = 30.4$ mm, 34.4 mm and 38.9 mm

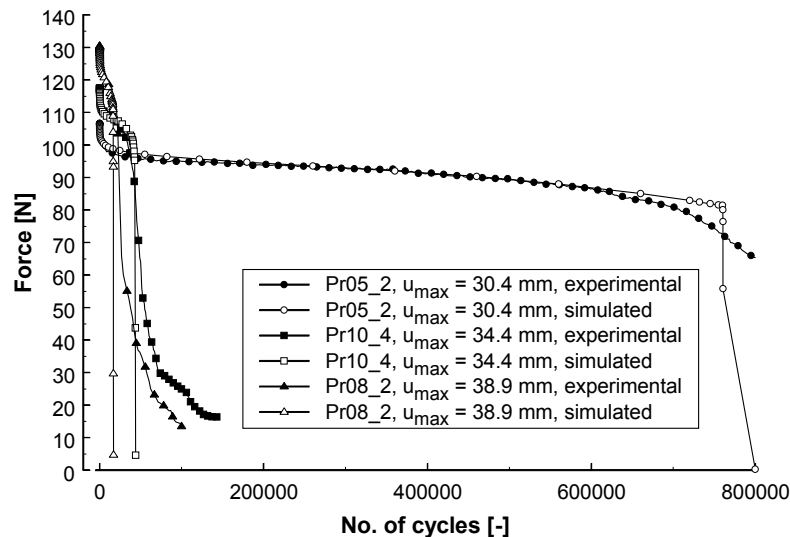


Figure 4 Experimental and simulated force-cycle histories for $[\#0^\circ]_8$ specimens in single-sided bending ($u_{\max} = 30.4$ mm, 34.4 mm and 38.9 mm) [30].

However, if applied to the bending fatigue tests of the $[\#45^\circ]_8$ stacking sequence, the one-dimensional nature of the model enforces only one stress component σ to be considered. So,

the normal stress σ_{xx} (in the bending direction) must be used in the constitutive equations, and no shear stresses can be taken into account. Figure 5 shows the finite element simulation for the $[\#45^\circ]_8$ specimen Pr06_1 ($u_{\max} = 35.6$ mm) with the one-dimensional fatigue damage model (4).

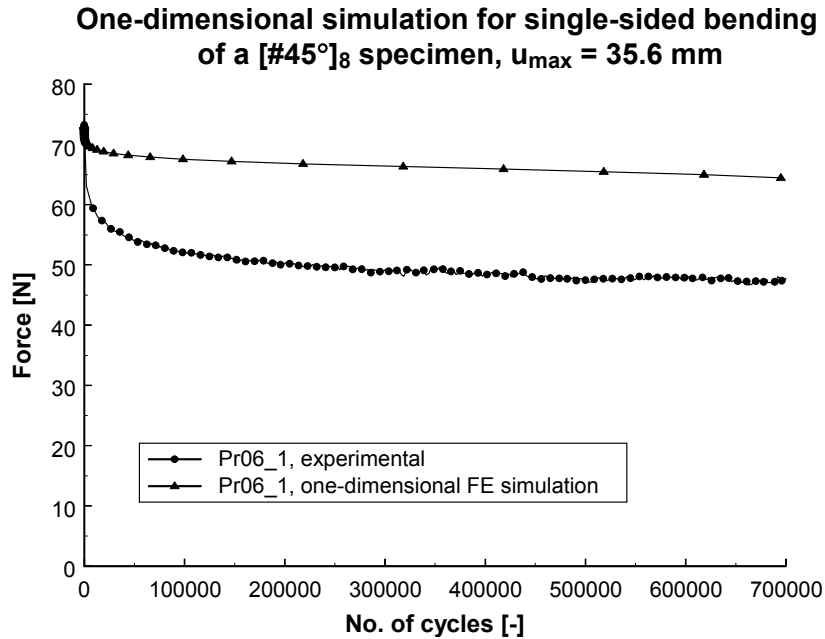


Figure 5 One-dimensional finite element simulation for $[\#45^\circ]_8$ specimen Pr06_1 with $u_{\max} = 35.6$ mm.

It is clear that the proposed one-dimensional fatigue damage law largely underestimates the force degradation under fatigue for the $[\#45^\circ]_8$ specimens. This is not surprising as the actual stress state in both stacking sequences is quite different. This is summarized in Figure 6.

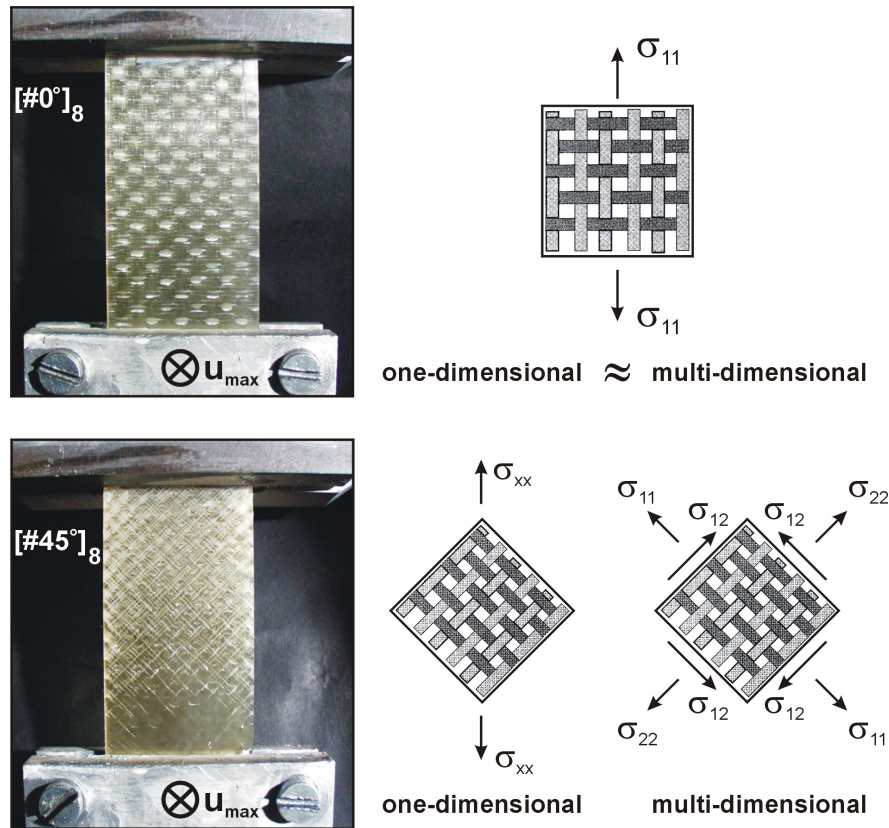


Figure 6 Schematical representation of the stress states in [#0°]₈ and [#45°]₈ specimens.

Indeed, in the [#0°]₈ stacking sequence, the only important orthotropic stress is σ_{11} and the bending load can be modelled as a quasi one-dimensional loading. Still supposing one-dimensional loading, the [#45°]₈ specimen with its fibres under an angle of 45° with the bending direction would be treated as a homogenized material with longitudinal stiffness E_{xx} , while in reality it is an orthotropic material with in-plane stiffness properties E_{11} , E_{22} , ν_{12} and G_{12} . In the [#45°]₈ stacking sequence, the orthotropic stresses σ_{11} , σ_{22} and σ_{12} all have comparable values (when normalized to their respective strengths) and are certainly not negligible one to another.

So, the one-dimensional fatigue damage model is not capable of simulating the fatigue behaviour of both [#0°]₈ and [#45°]₈ specimens with the same set of material constants. *This means that the model does not satisfy the demands of a true intrinsic material model, because the material constants of a true intrinsic material model could depend on the material type, but should certainly not depend on the loading state of the material.* As the stacking sequences [#45°]₈ and [#0°]₈ are two different lamination schemes of one and the same material, the same set of material constants should be used to predict the fatigue behaviour of both stacking sequences. Of course, it is evident that this one-dimensional model fails to do so, but it is important to draw the reader's attention to this crucial difference between intrinsic material models and non-intrinsic material models. And only true intrinsic material models can be applied successfully to full-scale composite structures, because, although the ply orientation and hence the stress state of each layer might be different, a true intrinsic material model can predict the fatigue behaviour of each material layer using the same set of material constants, independent of geometry and boundary conditions.

As a consequence, the extension of the present model to a multi-axial fatigue damage model that properly accounts for the different damage mechanisms in $[\#0^\circ]_8$ and $[\#45^\circ]_8$ composite specimens, is inevitable.

4. Multi-dimensional stress-strain-damage relationships

First it was investigated if the approximation of plane stress is valid for the considered loading conditions. Thereto, a nonlinear quasi-static finite element analysis of the first fatigue loading cycle (without fatigue damage) was performed for a few prescribed displacements u_{\max} .

Inspection of the three-dimensional stress state for the bending fatigue experiments proved that an in-plane treatment of the fatigue damage is justified. Indeed, the stacking sequence was chosen such that delaminations did not develop under the experimental loading conditions, and the out-of-plane stresses were very small. The normal stress component σ_{33} was compressive at the fixed clamp, due to the pre-tension force of the clamping plates, while its value was negligible remote from the fixed clamp. The value of the transverse shear component σ_{13} did not exceed 2.0 MPa for the largest prescribed displacements u_{\max} , while the in-plane stress components σ_{11} and σ_{22} reached values of more than 150 MPa.

Next, the extension of the one-dimensional fatigue damage model towards generalized in-plane loading conditions poses a very important problem: in the one-dimensional case, the relation between stress and strain was straightforward:

$$\sigma_{11} = E_0(1 - D_{11})\varepsilon_{11} \quad (5)$$

If the longitudinal Young's modulus E_0 is replaced by the stiffness matrix $[C]$, the relation $E = E_0(1 - D_{11})$ must be replaced by more complex relations including the interactions between several elastic properties. For example, Surgeon [36] reported a considerable degradation of the Poisson's ratio of cross-ply carbon/epoxy laminates under quasi-static tensile testing. This degradation has also been observed under fatigue loading.

To point out the difficulties with the transition from one-dimensional to multi-dimensional stress-strain-damage relations, the approaches proposed by Cauvin and Testa [37] and Lemaitre et al. [38] will be shortly reviewed first. It is important to discuss these approaches, because it will be shown that these approaches have been successfully applied to three-dimensional stress states in *metals*, but that their applicability to anisotropic fibre-reinforced composites is very limited.

Next, an alternative engineering approach will be proposed to establish the stress-strain-damage relationships, as it seemed that none of the existing theories in open literature could be used satisfactorily.

4.1. Stress-strain-damage relationships by Cauvin and Testa [37]

According to Cauvin and Testa [37], the three-dimensional equivalent of Equation (5) becomes:

$$\sigma_{ij} = \tilde{E}_{ijkl}\varepsilon_{kl} = (E_{ijkl} - D_{ijrs}E_{rskl})\varepsilon_{kl} \quad (6)$$

As the symmetry of the resulting stiffness tensor \tilde{E}_{ijkl} must be maintained, the damage tensor D_{ijrs} itself is not symmetric. Cauvin and Testa [37] have calculated that if the undamaged

material is *isotropic* and the damaged material is *orthotropic*, the damage tensor \mathbf{D} can be written as [37]:

$$\mathbf{D} = \begin{bmatrix} \mathbf{D}_{1111} & \mathbf{D}_{1122} & \mathbf{D}_{1133} & 0 & 0 & 0 \\ \mathbf{D}_{2211} & \mathbf{D}_{2222} & \mathbf{D}_{2233} & 0 & 0 & 0 \\ \mathbf{D}_{3311} & \mathbf{D}_{3322} & \mathbf{D}_{3333} & 0 & 0 & 0 \\ 0 & 0 & 0 & 2\mathbf{D}_{2323} & 0 & 0 \\ 0 & 0 & 0 & 0 & 2\mathbf{D}_{1313} & 0 \\ 0 & 0 & 0 & 0 & 0 & 2\mathbf{D}_{1212} \end{bmatrix} \quad (7)$$

Although this damage tensor is not symmetric, it still has only nine independent elements. Indeed, due to the required symmetry of $\tilde{\mathbf{E}}_{ijkl}$ (Eq. (6)), there are three constraint equations that relate the elements below the diagonal with the ones above [37] (these elements are in bold face):

$$\begin{aligned} \mathbf{D}_{2211} &= \mathbf{D}_{1122} + (\mathbf{D}_{1111} - \mathbf{D}_{2222}) \frac{\nu}{1-\nu} + (\mathbf{D}_{1133} - \mathbf{D}_{2233}) \frac{\nu}{1-\nu} \\ \mathbf{D}_{3311} &= \mathbf{D}_{1133} \frac{1-\nu+\nu^2}{1-\nu} + (\mathbf{D}_{1122} - \mathbf{D}_{3333})\nu + (\mathbf{D}_{1111} - \nu\mathbf{D}_{2222} - \mathbf{D}_{2233}) \frac{\nu}{1-\nu} \\ \mathbf{D}_{3322} &= \mathbf{D}_{2233} + (\mathbf{D}_{2222} - \mathbf{D}_{3333})\nu + (\mathbf{D}_{1122} - \mathbf{D}_{1133})\nu \end{aligned} \quad (8)$$

The Equations (8) have only been reported here to draw the reader's attention to the inevitable complexities when this scheme would be used to model stiffness degradation by fatigue:

- in the Equations (6) and (8), the elastic properties are only two in number: the *isotropic* Young's modulus E and the Poisson coefficient ν , because it was assumed that the undamaged material was isotropic. If this theory would be extended for fibre-reinforced composite materials with an initial orthotropic stiffness matrix, the constraint equations would be far more complex,
- nine damage growth rate equations should be established to predict the behaviour under fatigue of each of the nine independent elements of the damage tensor \mathbf{D} . Each of these equations would contain a few constants which would immediately raise the number of material constants to an unacceptable quantity for use in common practice,
- the simple relation between residual stiffness and damage in the one-dimensional case ($D = 1 - E/E_0$) has been replaced by complex equations relating the different damage variables with the different residual elastic properties.

Although this damage mechanics theory is mathematically consistent, it is too complicated for fatigue damage modelling of fibre-reinforced composites.

4.2. Stress-strain-damage relationships by Lemaitre et al. [38]

Another approach to solve the ambiguity of the non-symmetric damage tensor (see Equation (8)), is to use the stress as the dependent variable. Lemaitre et al. [38] calculated the strains as (summation convention):

$$\varepsilon_{ij}^e = \frac{1+\nu}{E} \tilde{\sigma}_{ij} - \frac{\nu}{E} \tilde{\sigma}_{kk} \delta_{ij} \quad (9)$$

where the effective stress tensor $\tilde{\sigma}_{ij}$ is symmetric and does not depend on the elasticity parameters (summation convention):

$$\tilde{\sigma}_{ij} = \left(H_{ik} \sigma_{kl}^{\text{Dev}} H_{lj} \right) + \frac{\sigma_H}{1 - \eta D_H} \delta_{ij} \quad (10)$$

$$\underline{H} = (\underline{1} - \underline{D})^{-1/2}$$

Without going into details, the effective stress tensor has been split up into a deviatoric stress σ^{Dev} (affected by a tensorial damage variable \underline{D}) and a hydrostatic stress σ_H (affected by the scalar damage variable D_H).

Further, Lemaitre et al. [38] needed a criterion to distinguish between tension and compression in multi-axial stress states, because the behaviour of micro-cracks in tension and compression was different. They proposed to calculate the principal stresses and to apply the crack closure coefficient h to the negative part of the principal stresses.

The approach outlined by Lemaitre et al. [38] is not suited for the fatigue modelling of fibre-reinforced composite materials, because of the following reasons:

- Lemaitre et al. [38] have applied the theory to the quasi-static behaviour of virgin isotropic steel alloys, not to the fatigue behaviour of virgin orthotropic composite materials. Although the theory may be sound for isotropic materials, it does not reflect the quite different mechanics of composite materials. Besides, the distinction between a deviatoric stress and a hydrostatic stress in Equation (10) is rather meaningless for fibre-reinforced composites, because the material is inhomogeneous and anisotropic, and the stress state depends on the fibre and matrix architecture,
- the elasticity law in Equation (9) poses serious difficulties when using implicit finite element codes, because the strains are function of the stresses.

4.3. *Alternative engineering approach for the stress-strain-damage relationships*

Here, an alternative engineering approach is proposed by the authors. It is first postulated that there is a distinct difference between the damage kinetics of intra-layer damage (matrix cracks, fibre/matrix debonding, fibre fracture,...) and inter-layer damage (delaminations). Moreover the responsible stress components are not the same. The in-plane stresses (σ_{11} , σ_{22} and σ_{12}) are affecting the intra-layer damage, while the out-of-plane stresses (σ_{13} , σ_{23} and σ_{33}) are causing inter-layer damage. It is clear that the one-dimensional fatigue damage model developed so far, is modelling the intra-layer damage types. Delaminations were not taken into account and the stacking sequence was chosen such that delaminations did not develop under the experimental loading conditions.

If only intra-layer damage is considered, it is postulated that there exist three damage variables D_{11} , D_{22} and D_{12} , which are defined through the relations:

$$\begin{Bmatrix} \sigma_{11} \\ \sigma_{22} \\ \sigma_{33} \\ \sigma_{23} \\ \sigma_{13} \\ \sigma_{12} \end{Bmatrix} = \begin{bmatrix} \sqrt{1-D_{11}} & 0 & 0 & 0 & 0 & 0 \\ 0 & \sqrt{1-D_{22}} & 0 & 0 & 0 & 0 \\ 0 & 0 & 1 & 0 & 0 & 0 \\ 0 & 0 & 0 & 1 & 0 & 0 \\ 0 & 0 & 0 & 0 & 1 & 0 \\ 0 & 0 & 0 & 0 & 0 & \sqrt{1-D_{12}} \end{bmatrix} \cdot \begin{bmatrix} C_{11} & C_{12} & C_{13} & 0 & 0 & 0 \\ C_{12} & C_{22} & C_{23} & 0 & 0 & 0 \\ C_{13} & C_{23} & C_{33} & 0 & 0 & 0 \\ 0 & 0 & 0 & C_{44} & 0 & 0 \\ 0 & 0 & 0 & 0 & C_{55} & 0 \\ 0 & 0 & 0 & 0 & 0 & C_{66} \end{bmatrix} \cdot \begin{Bmatrix} \varepsilon_{11} - \varepsilon_{11}^p \\ \varepsilon_{22} - \varepsilon_{22}^p \\ \varepsilon_{33} \\ 2\varepsilon_{23} \\ 2\varepsilon_{13} \\ 2\varepsilon_{12} \end{Bmatrix} \quad (11)$$

where $[C]$ is the initial orthotropic stiffness matrix of the composite material. The permanent strains ε_{11}^p and ε_{22}^p must account for the permanent deformation of the $[\#45^\circ]_8$ specimens (see Figure 3). Although this Equation represents a simplified approach, it is at least manageable in terms of number of damage variables and finite element implementation, because the symmetry of the stiffness matrix $[C]$ is guaranteed at any time during fatigue life.

A very important advantage of the formulation in Equation (11) is that the damage variables D_{11} , D_{22} and D_{12} are directly related with their respective stress components σ_{11} , σ_{22} and σ_{12} . As such, the damage growth rates dD_{11}/dN , dD_{22}/dN and dD_{12}/dN are driven by the respective stresses σ_{11} , σ_{22} and σ_{12} . In contrast, if for example the equation (6) would be used to define the damage variables D_{ijrs} , it would be very difficult to determine which stress components affect the growth rate of one particular damage variable D_{ijrs} , especially for the non-diagonal elements of the damage tensor. Further, there is a very clear distinction between positive and negative stresses for each of the damage variables. Indeed, for each damage variable, the sign of the corresponding stress component dictates which damage growth rate equation should be used, the one for tension or the one for compression. Finally, if the stress component changes sign during one fatigue loading cycle, the coupled differential equations for the corresponding tensile and compressive damage growth rate can be used [23].

Equation (11) can be worked out as follows:

$$\begin{Bmatrix} \sigma_{11} \\ \sigma_{22} \\ \sigma_{33} \\ \sigma_{23} \\ \sigma_{13} \\ \sigma_{12} \end{Bmatrix} = \begin{bmatrix} C_{11} \cdot (1-D_{11}) & C_{12} \cdot \sqrt{1-D_{11}} \cdot \sqrt{1-D_{22}} & C_{13} \cdot \sqrt{1-D_{11}} & 0 & 0 & 0 \\ C_{12} \cdot \sqrt{1-D_{11}} \cdot \sqrt{1-D_{22}} & C_{22} \cdot (1-D_{22}) & C_{23} \cdot \sqrt{1-D_{22}} & 0 & 0 & 0 \\ C_{13} \cdot \sqrt{1-D_{11}} & C_{23} \cdot \sqrt{1-D_{22}} & C_{33} & 0 & 0 & 0 \\ 0 & 0 & 0 & C_{44} & 0 & 0 \\ 0 & 0 & 0 & 0 & C_{55} & 0 \\ 0 & 0 & 0 & 0 & 0 & C_{66} \cdot (1-D_{12}) \end{bmatrix} \cdot \begin{Bmatrix} \varepsilon_{11} - \varepsilon_{11}^p \\ \varepsilon_{22} - \varepsilon_{11}^p \\ \varepsilon_{33} \\ 2\varepsilon_{23} \\ 2\varepsilon_{13} \\ 2\varepsilon_{12} \end{Bmatrix} \quad (12)$$

5. Discussion of the extended in-plane fatigue damage model

The one-dimensional fatigue damage model will now be extended for generalized in-plane loading conditions. The final objective is the development of a set of damage growth rate equations of the form:

$$\frac{dD_{11}}{dN} = \begin{cases} f_1(\sigma_{ij}, D_{ij}) & \text{if } \sigma_{11} \geq 0 \\ f_2(\sigma_{ij}, D_{ij}) & \text{if } \sigma_{11} < 0 \end{cases}$$

$$\frac{dD_{22}}{dN} = \begin{cases} g_1(\sigma_{ij}, D_{ij}) & \text{if } \sigma_{22} \geq 0 \\ g_2(\sigma_{ij}, D_{ij}) & \text{if } \sigma_{22} < 0 \end{cases} \quad (13)$$

$$\frac{dD_{12}}{dN} = h(\sigma_{ij}, D_{ij})$$

Each damage growth rate equation should depend on the multi-axial in-plane stress state σ_{ij} and the actual value of the damage variables D_{ij} . Further, additional equations for the growth rate of the permanent strains ε_{ii}^p ($i = 1,2$) must be established.

As each damage model should obey the Second Law of Thermodynamics, a few restrictions must be imposed upon the growth rate equations of damage and permanent strain. This is investigated first.

5.1. Second Law of Thermodynamics

Following the Second Law of Thermodynamics, it is investigated if the dissipated energy during each fatigue loading cycle is positive. This dissipated energy W_D is the work of the external forces minus the elastic energy, as the elastic energy is recovered during each fatigue loading cycle. So, the following condition must hold:

$$\dot{W}_D = \int_V \sigma_i \cdot \dot{\varepsilon}_i dV - \int_V \frac{d}{dt} \left(\frac{1}{2} \sigma_i \cdot \varepsilon_i^e \right) dV \geq 0 \quad (14)$$

If the established stress-strain relation (11) is written more generally as:

$$\sigma_i = \sqrt{1 - D_{ii}} \cdot C_{ij} \cdot \sqrt{1 - D_{jj}} \cdot \varepsilon_j^e \quad (i, j = 1, 2, \dots, 6) \quad (15)$$

whereby $\varepsilon_j^e = \varepsilon_j - \varepsilon_j^p$, Equation (14) can be worked out as follows:

$$\begin{aligned}
 \sigma_i \cdot \dot{\varepsilon}_i - \frac{d}{dt} \left(\frac{1}{2} \sigma_i \cdot \varepsilon_i^e \right) &= \frac{1}{2} \sigma_i \cdot \dot{\varepsilon}_i^e - \frac{1}{2} \dot{\sigma}_i \cdot \varepsilon_i^e + \sigma_i \cdot \dot{\varepsilon}_i^p \\
 &= \frac{1}{2} \sqrt{1-D_{ii}} \cdot C_{ij} \cdot \sqrt{1-D_{jj}} \cdot \varepsilon_j^e \cdot \dot{\varepsilon}_i^e + \frac{1}{4} \frac{\dot{D}_{ii}}{\sqrt{1-D_{ii}}} \cdot C_{ij} \cdot \sqrt{1-D_{jj}} \cdot \varepsilon_j^e \cdot \varepsilon_i^e \\
 &\quad + \frac{1}{4} \sqrt{1-D_{ii}} \cdot C_{ij} \cdot \frac{\dot{D}_{jj}}{\sqrt{1-D_{jj}}} \cdot \varepsilon_j^e \cdot \varepsilon_i^e - \frac{1}{2} \sqrt{1-D_{ii}} \cdot C_{ij} \cdot \sqrt{1-D_{jj}} \cdot \dot{\varepsilon}_j^e \cdot \varepsilon_i^e \\
 &\quad + \sigma_i \cdot \dot{\varepsilon}_i^p \\
 &= \frac{1}{4} \frac{\dot{D}_{ii}}{\sqrt{1-D_{ii}}} \cdot C_{ij} \cdot \sqrt{1-D_{jj}} \cdot \varepsilon_j^e \cdot \varepsilon_i^e \\
 &\quad + \frac{1}{4} \sqrt{1-D_{ii}} \cdot C_{ij} \cdot \frac{\dot{D}_{jj}}{\sqrt{1-D_{jj}}} \cdot \varepsilon_j^e \cdot \varepsilon_i^e + \sigma_i \cdot \dot{\varepsilon}_i^p
 \end{aligned} \tag{16}$$

The condition (14) is satisfied if $\dot{D}_{ii} \geq 0$ and $\sigma_i \cdot \dot{\varepsilon}_i^p \geq 0$. It will be clearly shown that the damage growth rate equations and the evolution law for the permanent strains satisfy these conditions.

5.2. Extended definition of the fatigue failure index Σ

Before presenting the damage growth rate equations, the one-dimensional formulation of the *fatigue failure index* $\Sigma(\sigma, D)$ (see Eq. (2)) must be extended. Thereto, the multi-axial in-plane stress state is taken into account by using the static Tsai-Wu failure criterion in its two-dimensional form [39]:

$$\frac{1}{X_T \cdot |X_C|} \sigma_{11}^2 + \frac{1}{Y_T \cdot |Y_C|} \sigma_{22}^2 + \frac{1}{S^2} \sigma_{12}^2 + \left(\frac{1}{X_T} - \frac{1}{|X_C|} \right) \sigma_{11} + \left(\frac{1}{Y_T} - \frac{1}{|Y_C|} \right) \sigma_{22} = 1 \tag{17}$$

where X_T and X_C are the tensile and compressive static strength in the material direction \vec{e}_{11} , Y_T and Y_C are the tensile and compressive static strength in the material direction \vec{e}_{22} , and S is the static shear strength. The static strength values for the plain woven glass/epoxy composite were listed in Table 2, and these values are used in all subsequent calculations.

In the original formulation of the Tsai-Wu static failure criterion, the interaction term $2F_{12}\sigma_{11}\sigma_{22}$ is also included in the criterion. In their basic papers on the Tsai-Wu static failure criterion, Tsai and Wu [39-40] calculated that F_{12} may be considered zero if it falls within the range $\pm 0.6 \times 10^{-4}$. These conclusions were based on the strength values measured for unidirectional graphite/epoxy specimens and it is now generally accepted that the influence of the F_{12} -term is often negligible. Narayanaswami and Adelman [41] have studied the tensor polynomial and Hoffman strength theories for composite materials and they as well concluded that the interaction coefficient is small, and can often be taken zero. It turned out that the zero-value for F_{12} was a good choice for the considered glass/epoxy material [30].

The *fatigue failure indices* Σ_{ij}^{2D} ($i, j = 1, 2$) for generalized in-plane fatigue loading can then be calculated from the Tsai-Wu static failure criterion (Eq. (17)) by replacing the nominal stresses σ_{ij} with the stresses $\sigma_{ij}/(1-D_{ij})$. The corresponding fatigue failure index Σ_{11}^{2D} for the stress component σ_{11} is defined as the positive root of the equation [30]:

$$\begin{aligned} & \left(\frac{1}{X_T} - \frac{1}{|X_C|} \right) \frac{\sigma_{11}}{\Sigma_{11}^{2D} \cdot (1-D_{11})} + \left(\frac{1}{Y_T} - \frac{1}{|Y_C|} \right) \frac{\sigma_{22}}{1-D_{22}} + \frac{1}{X_T \cdot |X_C|} \left(\frac{\sigma_{11}}{\Sigma_{11}^{2D} \cdot (1-D_{11})} \right)^2 \\ & + \frac{1}{Y_T \cdot |Y_C|} \left(\frac{\sigma_{22}}{1-D_{22}} \right)^2 + \frac{1}{S^2} \left(\frac{\sigma_{12}}{1-D_{12}} \right)^2 = 1 \end{aligned} \quad (18)$$

The fatigue failure index Σ_{22}^{2D} for the stress component σ_{22} is defined as the positive root of the equation [30]:

$$\begin{aligned} & \left(\frac{1}{X_T} - \frac{1}{|X_C|} \right) \frac{\sigma_{11}}{1-D_{11}} + \left(\frac{1}{Y_T} - \frac{1}{|Y_C|} \right) \frac{\sigma_{22}}{\Sigma_{22}^{2D} \cdot (1-D_{22})} + \frac{1}{X_T \cdot |X_C|} \left(\frac{\sigma_{11}}{1-D_{11}} \right)^2 \\ & + \frac{1}{Y_T \cdot |Y_C|} \left(\frac{\sigma_{22}}{\Sigma_{22}^{2D} \cdot (1-D_{22})} \right)^2 + \frac{1}{S^2} \left(\frac{\sigma_{12}}{1-D_{12}} \right)^2 = 1 \end{aligned} \quad (19)$$

Finally, the fatigue failure index Σ_{12}^{2D} for the stress component σ_{12} is defined as the positive root of the equation [30]:

$$\begin{aligned} & \left(\frac{1}{X_T} - \frac{1}{|X_C|} \right) \frac{\sigma_{11}}{1-D_{11}} + \left(\frac{1}{Y_T} - \frac{1}{|Y_C|} \right) \frac{\sigma_{22}}{1-D_{22}} + \frac{1}{X_T \cdot |X_C|} \left(\frac{\sigma_{11}}{1-D_{11}} \right)^2 \\ & + \frac{1}{Y_T \cdot |Y_C|} \left(\frac{\sigma_{22}}{1-D_{22}} \right)^2 + \frac{1}{S^2} \left(\frac{\sigma_{12}}{\Sigma_{12}^{2D} \cdot (1-D_{12})} \right)^2 = 1 \end{aligned} \quad (20)$$

These *fatigue failure indices* Σ_{11}^{2D} , Σ_{22}^{2D} and Σ_{12}^{2D} quantify the directional reserves to failure in in-plane loading conditions, taking into account the present damage state (D_{11} , D_{22} , D_{12}).

To assess the *relative importance of the separate stress components* σ_{ij} in the failure event, it is better to correlate the failure indices Σ_{ij}^{2D} ($i, j = 1, 2$) with their one-dimensional equivalent. Also, the failure indices must reduce to their one-dimensional equivalent if only one stress component is active.

A definition which satisfies these requirements, is the following:

$$\begin{aligned} \Sigma_{11} &= \frac{\Sigma_{11}^{2D}}{1 + (\Sigma_{11}^{2D} - \Sigma_{11}^{1D})} \\ \Sigma_{22} &= \frac{\Sigma_{22}^{2D}}{1 + (\Sigma_{22}^{2D} - \Sigma_{22}^{1D})} \\ \Sigma_{12} &= \frac{\Sigma_{12}^{2D}}{1 + (\Sigma_{12}^{2D} - \Sigma_{12}^{1D})} \end{aligned} \quad (21)$$

The failure indices Σ_{11}^{2D} , Σ_{22}^{2D} and Σ_{12}^{2D} are calculated from the respective equations (18), (19) and (20), while the one-dimensional failure indices Σ_{11}^{1D} , Σ_{22}^{1D} and Σ_{12}^{1D} are defined as the ratio of the effective stress $\tilde{\sigma}$ to the respective static strength (see Eq. (3)). So, the two-dimensional

failure indices Σ_{ij}^{2D} ($i, j = 1, 2$) take into account the adverse effect of multi-axial loading, while the correlation with the one-dimensional ratio Σ_{ij}^{1D} ($i, j = 1, 2$) to their respective static strengths indicates the relative probability of failure of each separate stress component. The newly defined failure indices Σ_{ij} reduce to their one-dimensional equivalent if a one-dimensional stress is applied, so the relation between one-dimensional and multi-dimensional failure indices remains consistent in use.

It is important to observe that if the stress state approaches the Tsai-Wu failure surface, not all failure indices Σ_{ij} ($i, j = 1, 2$) will approach the failure value 1.0, because the failure indices are normalized with respect to their one-dimensional ratio Σ_{ij}^{1D} ($i, j = 1, 2$). To avoid any singularities in the equations (18), (19) and (20) during fatigue life simulation, the calculation strategy is as follows:

- if one of the failure indices Σ_{ij} ($i, j = 1, 2$) has a high value, the corresponding damage variable D_{ij} will grow very rapidly,
- if this failure index Σ_{ij} approaches its failure value 1.0, the corresponding stress σ_{ij} is set to zero,
- in the next evaluation of the Tsai-Wu failure indices (Eqs. (18), (19) and (20)), all terms in the stress component σ_{ij} are set to zero and the corresponding damage D_{ij} is set to 1.0 for the remainder of the fatigue simulation.

A detailed discussion of the damage-dependent directional failure indices Σ_{ij} can be found in [42].

5.3. Accumulation of permanent strain

As already shown in Figure 3, the permanent deformation of the $[\#45^\circ]_8$ specimens can be considerable, and cannot be denied in this particular loading case. The problem however, is that there is almost no literature available on how this permanent deformation could be modelled for fibre-reinforced composites. Although the adequate modelling of this permanent strain phenomenon would require a research project on its own, an attempt is made to give at least an impression of the importance of this phenomenon for the considered loading case.

The proposed fatigue damage evolution law for the permanent strain is based on a rational modelling of the underlying damage kinetics, but cannot be based on a strong theoretical reasoning, because to the author's knowledge, the valuable information in open literature is very limited. However, a few assumptions might be justified:

- the permanent strain is related with the shear damage D_{12} , since the phenomenon is hardly observed with the $[\#0^\circ]_8$ specimens. Besides, the explanation is very plausible that matrix debris, formed by the shear stresses, is accumulated in the opening matrix cracks. It can therefore be assumed that the growth rate of the permanent strain is more or less proportional with the growth rate of the shear damage D_{12} ,
- the more the matrix cracks open during fatigue loading, the more matrix debris can be accumulated inside the cracks. The permanent strain growth rate in the \vec{e}_{11} and \vec{e}_{22} direction might therefore be proportional with the applied strain amplitude in the respective directions \vec{e}_{11} and \vec{e}_{22} ,
- as the cracks do not open at the compressive side, it is further accepted that the permanent strain does not grow if the applied stress is compressive,

- the possible effect of creep is not considered, because the test frequency was low (2.2 Hz) and the matrix was a thermosetting resin. Besides, no recovery of the permanent strain was observed after unloading, even not after one month. In case of creep, one would expect at least a small recovery after unloading.

Bearing in mind the above-mentioned considerations, the corresponding growth laws for the permanent strain have been written as (no summation convention) [30]:

$$\frac{d\varepsilon_{ii}^p}{dN} = \begin{cases} c_6 \cdot \varepsilon_{ii} \cdot \frac{dD_{12}}{dN} & \text{if } \sigma_{ii} \geq 0 \\ 0 & \text{if } \sigma_{ii} < 0 \end{cases} \quad (i = 1, 2) \quad (22)$$

The factor c_6 has been determined such that the predicted out-of-plane displacement profile after unloading matches the experimentally recorded one for the $[\#45^\circ]_8$ specimen Pr06_1 (see also Figure 5). This was the case for $c_6 = 0.6$. This implies that, if the damage D_{12} reaches its failure value 1.0, the permanent strain ε_{ii}^p cannot be larger than 60 % of the total strain amplitude ε_{ii} .

Figure 7 shows the experimental and simulated permanent deformation for the $[\#45^\circ]_8$ specimen Pr06_1 after having been subjected to 700,000 loading cycles with $u_{\max} = 35.6$ mm (see also Figure 5). The irregular shape of the experimentally measured out-of-plane displacement profile is due to the recording technique. The deformation has been extracted from a digitally recorded image with the edge detection algorithm [30], and as each pixel has a finite width, the shape is not very smooth. This effect is aggravated by the very small scale of the permanent deformation which is only a few millimeters large.

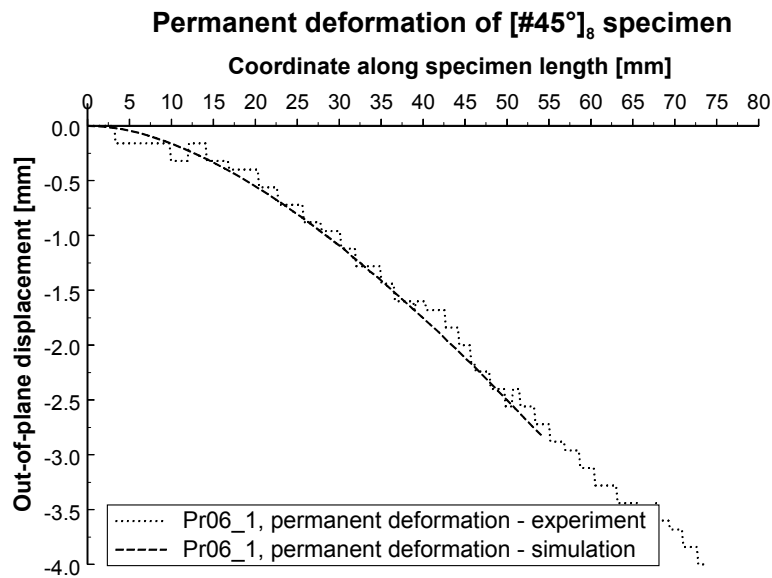


Figure 7 Experimental and predicted permanent deformation of $[\#45^\circ]_8$ specimen Pr06_1 after 700,000 loading cycles ($u_{\max} = 35.6$ mm).

5.4. Layout of the constitutive equations

In this paragraph, all relevant equations of the fatigue damage model for generalized in-plane fatigue loading conditions are brought together in a consistent framework. The stress-strain-damage relationships were already defined in Equation (11) and the evolution laws $d\epsilon_{11}^p/dN$ and $d\epsilon_{22}^p/dN$ were defined in the previous paragraph. Now the damage growth rate equations dD_{11}/dN , dD_{22}/dN and dD_{12}/dN must be established.

The one-dimensional fatigue damage model for single-sided bending, as it was defined in Equation (4), should remain valid without any modification of the parameter values c_i ($i = 1, \dots, 5$) for the damage growth rate in the material coordinate directions \vec{e}_{11} and \vec{e}_{22} , because the plain woven glass fabric is balanced in the warp and weft directions. The only modifications allowed are the replacement of the one-dimensional fatigue failure index Σ by the multi-dimensional fatigue failure indices Σ_{11} and Σ_{22} , and the replacement of the damage variable D by the damage variables D_{11} and D_{22} .

Furthermore, it is assumed for the moment that the growth rate equation dD_{12}/dN has the same structure as the growth rate equation for tensile damage, because the shear stress causes fibre/matrix debonding and this damage type has been identified as the initiating mechanism for transverse cracking [43]. Finally, as the sign of the orthotropic shear stress σ_{12} does not affect the damage evolution, there is no discrimination between positive and negative shear stresses.

$$\frac{dD_{11}}{dN} = \begin{cases} c_1 \cdot \Sigma_{11} \cdot \exp\left(-c_2 \frac{D_{11}}{\sqrt{\Sigma_{11}}}\right) + c_3 \cdot D_{11} \cdot \Sigma_{11}^2 \cdot [1 + \exp(c_5(\Sigma_{11} - c_4))] & \text{if } \sigma_{11} \geq 0 \\ \left[c_1 \cdot \Sigma_{11} \cdot \exp\left(-c_2 \frac{D_{11}}{\sqrt{\Sigma_{11}}}\right) \right]^3 + c_3 \cdot D_{11} \cdot \Sigma_{11}^2 \cdot \left[1 + \exp\left(\frac{c_5}{3}(\Sigma_{11} - c_4)\right) \right] & \text{if } \sigma_{11} < 0 \end{cases}$$

$$\frac{dD_{22}}{dN} = \begin{cases} c_1 \cdot \Sigma_{22} \cdot \exp\left(-c_2 \frac{D_{22}}{\sqrt{\Sigma_{22}}}\right) + c_3 \cdot D_{22} \cdot \Sigma_{22}^2 \cdot [1 + \exp(c_5(\Sigma_{22} - c_4))] & \text{if } \sigma_{22} \geq 0 \\ \left[c_1 \cdot \Sigma_{22} \cdot \exp\left(-c_2 \frac{D_{22}}{\sqrt{\Sigma_{22}}}\right) \right]^3 + c_3 \cdot D_{22} \cdot \Sigma_{22}^2 \cdot \left[1 + \exp\left(\frac{c_5}{3}(\Sigma_{22} - c_4)\right) \right] & \text{if } \sigma_{22} < 0 \end{cases} \quad (23)$$

$$\frac{dD_{12}}{dN} = c_1 \cdot \Sigma_{12} \cdot \exp\left(-c_2 \frac{D_{12}}{\sqrt{\Sigma_{12}}}\right) + c_3 \cdot D_{12} \cdot \Sigma_{12}^2 \cdot [1 + \exp(c_5(\Sigma_{12} - c_4))]$$

It appears that this set of equations was not able to simulate the bending fatigue results of the $[\#45^\circ]_8$ specimens. After a close inspection of the damage growth rate equations and the experimental observations, it was concluded that two modifications were necessary [30]:

- the growth rate equations for D_{11} , D_{22} and D_{12} had to be coupled,
- the damage evolution law dD_{12}/dN had to be modified.

It is obvious that all modifications contribute to the enhanced agreement between experiment and simulation, and that these modifications affect each other. Indeed, if the growth rate equation dD_{12}/dN is changed (both initiation and propagation), the values of D_{11} and D_{22} are affected through the coupling terms with D_{12} , and the growth rate $d(\epsilon_{ii}^p)/dN$ is proportional with the growth rate dD_{12}/dN . Therefore a large number of simulations have been made before the simultaneous effect of these modifications resulted in good predictions of the force-cycle history. Further, all modifications have proved to be essential, in order to obtain good simulations for a wide range of prescribed displacements u_{max} .

A detailed study of these modifications can be found in [30]. In the end the close feedback between experimental observations and finite element predictions has lead to the final damage growth rate equations for generalized in-plane fatigue loading [30]:

$$\frac{dD_{11}}{dN} = \begin{cases} c_1 \cdot (1 + D_{12}^2) \cdot \Sigma_{11} \cdot \exp\left(-c_2 \frac{D_{11}}{\sqrt{\Sigma_{11}} \cdot (1 + D_{12}^2)}\right) & \text{if } \sigma_{11} \geq 0 \\ + c_3 \cdot D_{11} \cdot \Sigma_{11}^2 \cdot [1 + \exp(c_5(\Sigma_{11} - c_4))] & \\ \left[c_1 \cdot (1 + D_{12}^2) \cdot \Sigma_{11} \cdot \exp\left(-c_2 \frac{D_{11}}{\sqrt{\Sigma_{11}} \cdot (1 + D_{12}^2)}\right) \right]^{1+2 \cdot \exp(-D_{12})} & \text{if } \sigma_{11} < 0 \\ + c_3 \cdot D_{11} \cdot \Sigma_{11}^2 \cdot \left[1 + \exp\left(\frac{c_5}{3}(\Sigma_{11} - c_4)\right) \right] & \end{cases}$$

$$\frac{dD_{22}}{dN} = \begin{cases} c_1 \cdot (1 + D_{12}^2) \cdot \Sigma_{22} \cdot \exp\left(-c_2 \frac{D_{22}}{\sqrt{\Sigma_{22}} \cdot (1 + D_{12}^2)}\right) & \text{if } \sigma_{22} \geq 0 \\ + c_3 \cdot D_{22} \cdot \Sigma_{22}^2 \cdot [1 + \exp(c_5(\Sigma_{22} - c_4))] & \\ \left[c_1 \cdot (1 + D_{12}^2) \cdot \Sigma_{22} \cdot \exp\left(-c_2 \frac{D_{22}}{\sqrt{\Sigma_{22}} \cdot (1 + D_{12}^2)}\right) \right]^{1+2 \cdot \exp(-D_{12})} & \text{if } \sigma_{22} < 0 \\ + c_3 \cdot D_{22} \cdot \Sigma_{22}^2 \cdot \left[1 + \exp\left(\frac{c_5}{3}(\Sigma_{22} - c_4)\right) \right] & \end{cases}$$

$$\frac{dD_{12}}{dN} = c_1 \cdot \Sigma_{12} \cdot \exp\left(-c_2 \frac{D_{12}}{2\sqrt{\Sigma_{12}}}\right) \quad (24)$$

The equations (11), (22) and (24) make up the complete system of constitutive equations to simulate single-sided bending. This system of equations will further be validated by finite element simulations of the fatigue behaviour of the $[\#45^\circ]_8$ specimens.

Finally, it is important to observe that the multi-axial fatigue damage model reduces perfectly to its one-dimensional equivalent (Eq. (4)) if a uni-axial fatigue loading is applied. Indeed, if only one stress component $\sigma_{11} = \sigma$ is acting, the Tsai-Wu static failure criterion reduces to its one-dimensional formulation (2) and the fatigue failure indices $(\Sigma_{11}, \Sigma_{22}, \Sigma_{12})$ convert to $(\Sigma, 0, 0)$. As a consequence, only the damage growth rate dD_{11}/dN is not zero and converts to

the one-dimensional equation (4). The stress-strain relationship (11) reduces to the simple relation (1) and the increments $d\varepsilon_{ii}^p/dN$ of permanent strain are zero, because dD_{12}/dN is zero. As such, there is a perfect transition from the multi-dimensional model to the one-dimensional model and vice-versa.

5.5. Finite element implementation

The complete fatigue model has been implemented in the commercial finite element code SAMCEF™. The composite specimen has been modelled with solid brick elements and much attention has been paid to the correct finite element modelling of the fixed clamp and the boundary conditions [44]. Following the developed *cycle jump* approach [45], the finite element calculation starts with the simulation of the first fatigue loading cycle. Next, the increments of damage and permanent strain are calculated for each Gauss-point of the composite specimen. Then it is calculated how many cycles can be jumped over without losing accuracy on the most damaging Gauss-points. Finally, the calculation is restarted for a new loading cycle with altered damage and stiffness properties for each Gauss-point.

6. Finite element simulations

Now that the final multi-axial growth rate equations have been established for single-sided bending, the experimental results of the Pr06_1 fatigue test (see Figure 5) are used to investigate in more detail the output of the finite element simulation.

Figure 8 shows the finite element simulation for the $[\#45^\circ]_8$ specimen Pr06_1 with the application of the complete system of equations (11), (22) and (24). The simulation without permanent strain has been included here for comparison purpose.

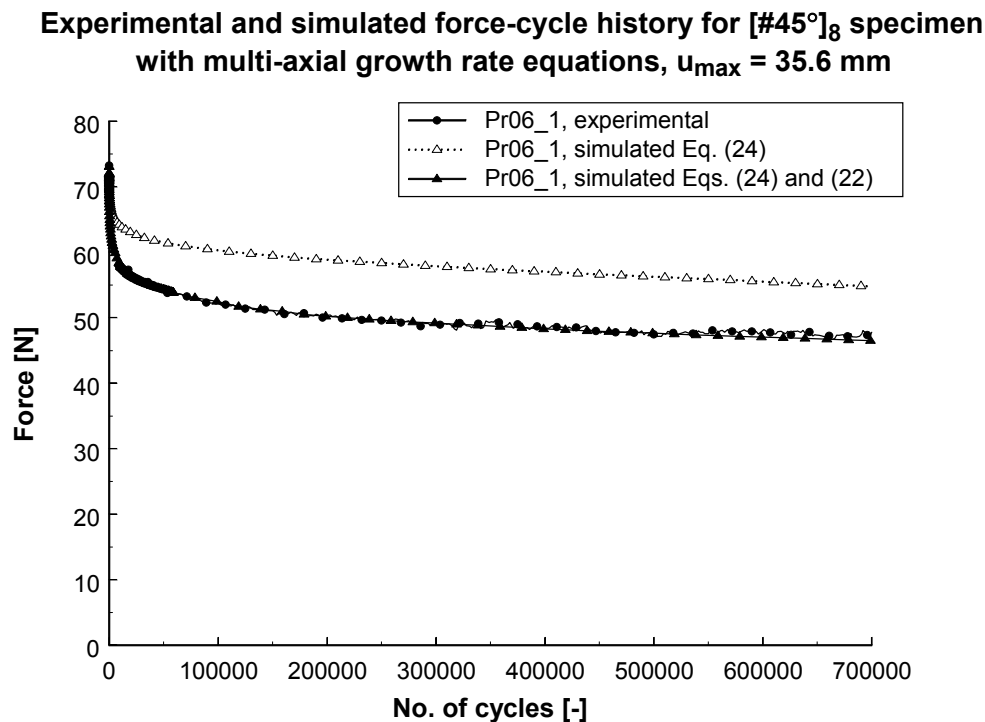


Figure 8 Experimental and simulated force-cycle history for $[\#45^\circ]_8$ specimen Pr06_1 with application of the damage growth rate equations (24) and with/without permanent strain (22).

As can be seen from Figure 8, the agreement is now very good. If the simulated force-cycle histories with and without permanent strain in Figure 8 are compared, it is clear that the permanent strain considerably affects the force-cycle history and cannot be ignored in the modelling stage.

Figure 9 shows the cycle history of the damage variables D_{11} , D_{22} and D_{12} for the Gauss-point 1544, which is situated in the clamped cross-section, halfway between the midplane and the tensile surface. Figure 10 shows the cycle history of the corresponding fatigue failure indices Σ_{11} , Σ_{22} and Σ_{12} for the same Gauss-point 1544. Only the first 100,000 loading cycles (compared to Figure 8) have been shown to make the initiation phase more visible on the graph. After 100,000 loading cycles, the degradation occurs very gradually and little change can be seen in the calculated damage and failure index values.

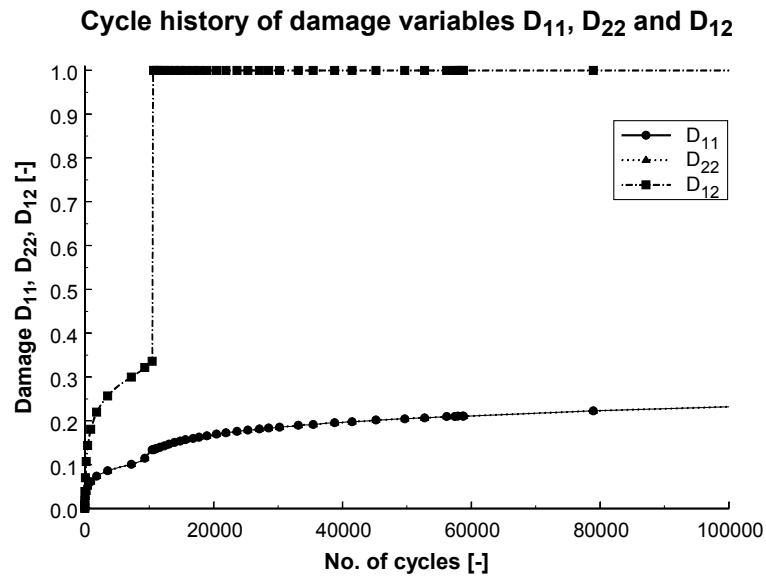


Figure 9 Cycle history of the damage variables D_{11} , D_{22} and D_{12} for the Gauss-point 1544 ($[\#45^\circ]_8$ specimen Pr06_1, $u_{\max} = 35.6$ mm).

The curves of the damage variables D_{11} and D_{22} are coincident, since the principal material axes \vec{e}_{11} and \vec{e}_{22} of the $[\#45^\circ]_8$ specimens are situated symmetrically with respect to the bending direction. Hence the stresses σ_{11} and σ_{22} have the same value, and the damage growth rates dD_{11}/dN and dD_{22}/dN are exactly the same.

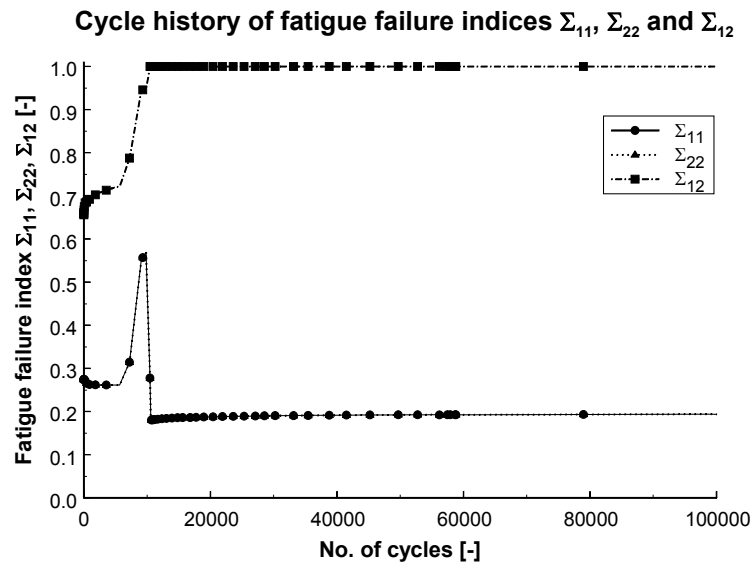


Figure 10 Cycle history of the fatigue failure indices Σ_{11} , Σ_{22} and Σ_{12} for the Gauss-point 1544 ($[\#45^\circ]_8$ specimen Pr06_1, $u_{\max} = 35.6$ mm).

At early fatigue loading, the shear damage D_{12} is growing fast, resulting in an increasing effective stress $\tilde{\sigma}_{12}$ ($= \sigma_{12}/(1-D_{12})$) and fatigue failure index Σ_{12} . The fatigue failure indices Σ_{11} and Σ_{22} on the other hand, are slightly decreasing. On first thoughts this seems unexpected because (i) the increasing effective stress $\tilde{\sigma}_{12}$ results in a more harmful stress state $(\tilde{\sigma}_{11}, \tilde{\sigma}_{22}, \tilde{\sigma}_{12})$ and thus higher fatigue failure indices Σ_{ij} , and (ii) the damage variables D_{11} and D_{22} are increasing as well. However, the decrease of Σ_{11} and Σ_{22} is due to the accumulation of permanent strain. Being largely affected by the growth rate dD_{12}/dN , the permanent strains are accumulating fast (see Eq. (22)) and the corresponding nominal stresses σ_{11} and σ_{22} are decreasing. The combined effect of (i) increasing damage D_{11} and D_{22} and (ii) accumulation of permanent strain results in lower nominal stresses σ_{11} and σ_{22} and slightly decreasing fatigue failure indices Σ_{11} and Σ_{22} .

Once the fatigue failure index Σ_{12} approaches failure, the corresponding damage D_{12} is set to its failure value 1.0. As $\tilde{\sigma}_{12}$ is set to zero in the Tsai-Wu failure criterion after the failure of Σ_{12} , the stress state $(\tilde{\sigma}_{11}, \tilde{\sigma}_{22})$ is less critical than the former stress state $(\tilde{\sigma}_{11}, \tilde{\sigma}_{22}, \tilde{\sigma}_{12})$, and hence the fatigue failure indices Σ_{11} and Σ_{22} reduce by about 60 %. As a consequence, the damage growth rates dD_{11}/dN and dD_{22}/dN are slowing down very fast. Further, due to the presence of permanent strain, the nominal stresses remain very small. This state of very slow damage propagation is gradually reached for all Gauss-points, and this explains why the experimentally measured force-cycle history in Figure 8 is quasi horizontal after a certain fatigue loading time.

Finally, Figure 11 shows the experimental and simulated force-cycle history for the Pr04_5 specimen, subjected to the prescribed displacement $u_{\max} = 32.3$ mm.

**Experimental and simulated force-cycle history for $[\#45^\circ]_8$ specimen
single-sided bending, $u_{\max} = 32.3$ mm**

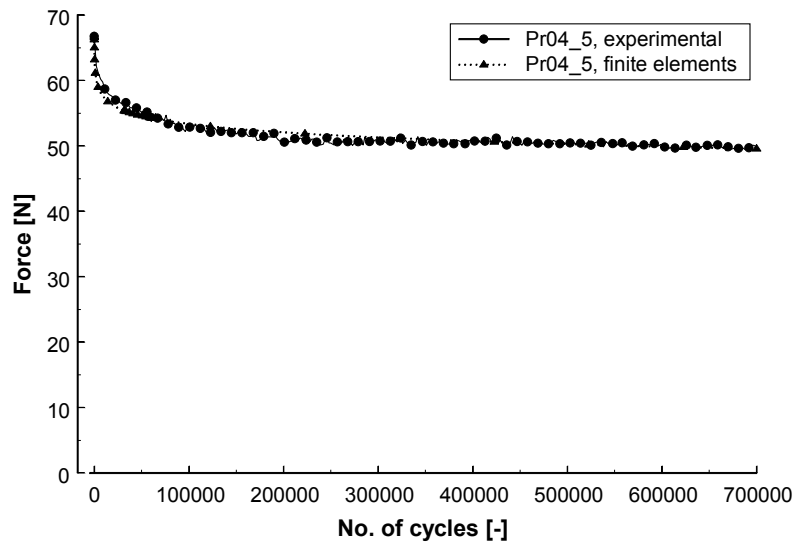


Figure 11 Experimental and simulated force-cycle history for the $[\#45^\circ]_8$ specimen Pr04_5 ($u_{\max} = 32.3$ mm).

An in-depth validation of the multi-axial fatigue model for the $[\#45^\circ]_8$ laminates can be found in [30]. Although the emphasis in the present paper lies on the theoretical modelling framework, it can be concluded that this multi-axial fatigue model for single-sided bending can simulate the experimental results for the $[\#45^\circ]_8$ specimens, including stiffness degradation and permanent strain, while the constants c_i ($i = 1, \dots, 5$) have been retained from the one-dimensional fatigue damage model.

7. Conclusions

Displacement-controlled bending fatigue tests were performed on both $[\#0^\circ]_8$ and $[\#45^\circ]_8$ glass/epoxy specimens. A previously developed one-dimensional fatigue model could simulate the observed results for the $[\#0^\circ]_8$ specimens very well, but not those for the $[\#45^\circ]_8$ specimens, if the material constants c_i were retained. Especially the large initial decrease of the bending force and the accumulation of permanent strain of the $[\#45^\circ]_8$ specimens required a multi-axial formulation of the residual stiffness model. To that purpose, the multi-dimensional stress-strain-damage relationships were established and a new evolution law for the permanent strains was developed. Finally the damage growth rate equations were defined. Together, all these equations constitute the framework for the multi-axial residual stiffness model that is capable of simulating stiffness degradation, stress redistribution and permanent strain in the $[\#45^\circ]_8$ specimens.

It is also important to observe that the framework is very general in nature and can be applied to a wide range of fibre-reinforced composites. Other failure criteria than Tsai-Wu can be used and different damage growth rate equations can be established, but the concept of the fatigue failure indices, the structure of the damage evolution laws and the global relations between stress, strain, damage and permanent strain might be valid for a broader class of composites.

Acknowledgements

The author W. Van Paepegem gratefully acknowledges his finance through a grant of the Fund for Scientific Research – Flanders (F.W.O.), and the advice and technical support of the SAMTECH company. The authors also express their gratitude to Syncoglas for their support and technical collaboration.

References

[1]	Degrieck, J. and Van Paepegem, W. (2001). Fatigue Damage Modelling of Fibre-Reinforced Composite Materials: Review. <i>Applied Mechanics Reviews</i> , 54(4), 279-300.
[2]	Lawrence Wu, C.M. (1993). Thermal and mechanical fatigue analysis of CFRP laminates. <i>Composite Structures</i> , 25, 339-344.
[3]	Jen, M.-H.R. and Lee, C.-H. (1998). Strength and life in thermoplastic composite laminates under static and fatigue loads. Part I: Experimental. <i>International Journal of Fatigue</i> , 20(9), 605-615.
[4]	Jen, M.-H.R. and Lee, C.-H. (1998). Strength and life in thermoplastic composite laminates under static and fatigue loads. Part II: Formulation. <i>International Journal of Fatigue</i> , 20(9), 617-629.
[5]	Philippidis, T.P. and Vassilopoulos, A.P. (1999). Fatigue strength prediction under multiaxial stress. <i>Journal of Composite Materials</i> , 33(17), 1578-1599.
[6]	Talreja, R. (1986). Stiffness properties of composite laminates with matrix cracking and interior delamination. <i>Engineering Fracture Mechanics</i> , 25(5/6), 751-762.
[7]	Talreja, R. (1990). Damage mechanics of composite materials based on thermodynamics with internal variables. In : Cardon, A.H. and Verchery, G. (eds.). <i>Durability of polymer based composite systems for structural applications. Proceedings of the International Colloquium, 27-31 August 1990, Brussels, Belgium, Elsevier</i> , pp. 65-79.
[8]	Talreja, R., Yalvac, S., Yats, L.D. and Wetters, D.G. (1992). Transverse cracking and stiffness reduction in cross-ply laminates of different matrix toughness. <i>Journal of Composite Materials</i> , 26(11), 1644-1663.
[9]	Allen, D.H., Harris, C.E. and Groves, S.E. (1987). A thermomechanical constitutive theory for elastic composites with distributed damage - I. Theoretical development. <i>International Journal of Solids and Structures</i> , 23(9), 1301-1318.
[10]	Allen, D.H., Harris, C.E. and Groves, S.E. (1987). A thermomechanical constitutive theory for elastic composites with distributed damage - II. Application to matrix cracking in laminated composites. <i>International Journal of Solids & Structures</i> , 23(9), 1319-1338.
[11]	Allen, D.H., Highsmith, A.L. and Lo, D.C. (1990). A continuum damage mechanics model for life prediction of laminated composites. In : Cardon, A.H. and Verchery, G. (eds.). <i>Durability of polymer based composite systems for structural applications. Proceedings of the International Colloquium, 27-31 August 1990, Brussels, Belgium, Elsevier</i> , pp. 119-128.
[12]	Lee, J.-W., Allen, D.H. and Harris, C.E. (1989). Internal state variable approach for predicting stiffness reductions in fibrous laminated composites with matrix cracks. <i>Journal of Composite Materials</i> , 23, 1273-1291.
[13]	Sedrakian, A., Ben Zineb, T., Billoet, J.L., Sicot, N. and Lardeur, P. (1997). A numerical model of fatigue behaviour for composite plates: application to a three point bending test. In : Degallaix, S., Bathias, C. and Fougères, R. (eds.). <i>International Conference on fatigue of composites. Proceedings, 3-5 June 1997, Paris, France, La Société Française de Métallurgie et de Matériaux</i> , pp. 415-423.
[14]	Sedrakian, A., Ben Zineb, T., Billoet, J.L. and Bobet, V. (2000). Fatigue behaviour simulation of industrial composite parts. In: <i>Proceedings of the Second International Conference on Fatigue of Composites. 4-7 June 2000, Williamsburg</i> , pp. 4.5-4.6.
[15]	Shokrieh, M.M. and Lessard, L.B. (1997). Multiaxial fatigue behaviour of unidirectional plies based on uniaxial fatigue experiments - I. Modelling. <i>International Journal of Fatigue</i> , 19(3), 201-207.
[16]	Shokrieh, M.M. and Lessard, L.B. (1997). Multiaxial fatigue behaviour of unidirectional plies based on uniaxial fatigue experiments - II. Experimental evaluation. <i>International Journal of Fatigue</i> , 19(3), 209-217.
[17]	Shokrieh, M.M. and Lessard, L.B. (1998). Residual fatigue life simulation of laminated composites. In : Gowayed, Y. and Abd El Hady, F. (eds.). <i>Proceedings of the International Conference on Advanced</i>

	Composites (ICAC 98), 15-18 December 1998, Hurghada, Egypt, pp. 79-86.
[18]	Shokrieh, M.M. (1996). Progressive fatigue damage modelling of composite materials. Ph.D. Thesis, McGill University, Montréal, Canada.
[19]	Shokrieh, M.M. and Lessard, L.B. (2000). Progressive fatigue damage modeling of composite materials, Part I: Modeling. <i>Journal of Composite Materials</i> , 34(13), 1056-1080.
[20]	Shokrieh, M.M. and Lessard, L.B. (2000). Progressive fatigue damage modeling of composite materials, Part II: Material characterization and model verification. <i>Journal of Composite Materials</i> , 34(13), 1081-1116.
[21]	Degrieck, J., Van Paepegem, W. and Boone, P. (2001). Application of digital phase-shift shadow Moiré to micro deformation measurements of curved surfaces. <i>Optics and Lasers in Engineering</i> , 36, 29-40.
[22]	Van Paepegem, W. and Degrieck, J. (2001). Fatigue Degradation Modelling of Plain Woven Glass/epoxy Composites. <i>Composites Part A</i> , 32(10), 1433-1441.
[23]	Van Paepegem, W. and Degrieck, J. (2002). Tensile and Compressive Damage Coupling for Fully-reversed Bending Fatigue of Fibre-reinforced Composites. <i>Fatigue and Fracture of Engineering Materials & Structures</i> , 25(6), 547-562.
[24]	Sol, H. and de Wilde, W.P. (1988). Identification of elastic properties of composite materials using resonant frequencies. In : Brebbia, C.A., de Wilde, W.P. and Blain, W.R. (eds.). <i>Proceedings of the International Conference "Computer Aided Design in Composite Material Technology"</i> , Southampton, 1988, Springer-Verlag, pp. 273-280.
[25]	Sol, H. (1990). Identification of the complex moduli of composite materials by a mixed numerical/experimental method. In : de Wilde, W.P. and Blain, W.R. (eds.). <i>Proceedings of the second International Conference on Computer Aided Design in Composite Material Technology</i> , Brussels, 25-27 April 1990, Springer-Verlag, pp. 267-279.
[26]	Wevers, M., Verpoest, I., Aernoudt, E. and De Meester, P. (1987). Fatigue damage development in carbon fiber reinforced epoxy composites: correlation between the stiffness degradation and the growth of different damage types. In : Matthews, F.L. et al. (eds.). <i>Sixth International Conference on Composite Materials (ICCM-VI) & Second European Conference on Composite Materials (ECCM-II) : Volume 4. Proceedings, 20-24 July 1987, London, UK, Elsevier</i> , pp. 4.114-4.128.
[27]	Wevers, M., Verpoest, I. and De Meester, P. (1990). Is crack closure due to fatigue loading causing more damage in carbon fibre reinforced epoxy composites ? In : Füller, J. et al. (eds.). <i>ECCM-4 : Developments in the science and technology of composite materials. Proceedings of the Fourth European Conference on Composite Materials, 25-28 September, Stuttgart, Germany, Elsevier</i> , pp. 181-188.
[28]	Van Paepegem, W. and Degrieck, J. (2002). A New Coupled Approach of Residual Stiffness and Strength for Fatigue of Fibre-reinforced Composites. <i>International Journal of Fatigue</i> , 24(7), 747-762.
[29]	Van Paepegem, W. and Degrieck, J. (2002). Coupled Residual Stiffness and Strength Model for Fatigue of Fibre-reinforced Composite Materials. <i>Composites Science and Technology</i> , 62(5), 687-696.
[30]	Van Paepegem, W. (2002). Development and finite element implementation of a damage model for fatigue of fibre-reinforced polymers. Ph.D. thesis. Ghent, Ghent University Architectural and Engineering Press (ISBN 90-76714-13-4), 403 p.
[31]	Van Paepegem, W. and Degrieck, J. (2002). Modelling single-sided and fully-reversed bending fatigue of fibre-reinforced composites. <i>Proceedings of the Tenth European Conference on Composite Materials (ECCM-10), Brugge, Belgium, 3-7 June 2002</i> , pp. 1-8.
[32]	Schulte, K. (1984). Stiffness reduction and development of longitudinal cracks during fatigue loading of composite laminates. In : Cardon, A.H. and Verchery, G. (eds.). <i>Mechanical characterisation of load bearing fibre composite laminates. Proceedings of the European Mechanics Colloquium 182, 29-31 August 1984, Brussels, Belgium, Elsevier</i> , pp. 36-54.
[33]	Highsmith, A.L. and Reifsnider, K.L. (1982). Stiffness-reduction mechanisms in composite laminates. In : Reifsnider, K.L. (ed.). <i>Damage in composite materials. ASTM STP 775. American Society for Testing and Materials</i> , pp. 103-117.
[34]	Masters, J.E. and Reifsnider, K.L. (1982). An investigation of cumulative damage development in quasi-isotropic graphite/epoxy laminates. In : Reifsnider, K.L. (ed.). <i>Damage in composite materials. ASTM STP 775. American Society for Testing and Materials</i> , pp. 40-62.
[35]	Van Paepegem, W. and Degrieck, J. (2002). Effects of Load Sequence and Block Loading on the Fatigue Response of Fibre-reinforced Composites. <i>Mechanics of Composite Materials and Structures</i> , 9(1), 19-35.
[36]	Surgeon, M. (1999). Continuous damage monitoring techniques for laminated CFRP composite

	materials. Doctoral thesis. Leuven, Katholieke Universiteit Leuven, pp. 178-204.
[37]	Cauvin, A. and Testa, R.B. (1999). Damage mechanics : basic variables in continuum theories. <i>International Journal of Solids & Structures</i> , 36, 747-761.
[38]	Lemaitre, J., Desmorat, R. and Sauzay, M. (2000). Anisotropic damage law of evolution. <i>European Journal of Mechanics A/Solids</i> , 19, 187-208.
[39]	Tsai, S.W. and Wu, E.M. (1971). A general theory of strength for anisotropic materials. <i>Journal of Composite Materials</i> , 5, 58-80.
[40]	Wu, E.M. (1972). Optimal experimental measurements of anisotropic failure tensors. <i>Journal of Composite Materials</i> , 6, 472-489.
[41]	Narayanaswami, R. and Adelman, H.M. (1977). Evaluation of the tensor polynomial and Hoffman strength theories for composite materials. <i>Journal of Composite Materials</i> , 11, 366-377.
[42]	Van Paepegem, W. and Degrieck, J. (2002). Calculation of Damage-dependent Directional Failure Indices from the Tsai-Wu Static Failure Criterion. <i>Composites Science and Technology</i> , in press.
[43]	Gamstedt, E.K. and Sjogren, B.A. (1999). Micromechanisms in tension-compression fatigue of composite laminates containing transverse plies. <i>Composites Science and Technology</i> , 59(2), 167-178.
[44]	Van Paepegem, W. and Degrieck, J. (2001). Modelling strategies for fatigue damage behaviour of fibre-reinforced composites. <i>European Journal of Mechanical and Environmental Engineering</i> , 46(4), 217-227.
[45]	Van Paepegem, W., Degrieck, J. and De Baets, P. (2001). Finite Element Approach for Modelling Fatigue Damage in Fibre-reinforced Composite Materials. <i>Composites Part B</i> , 32(7), 575-588.